



Using micro-ct to investigate nanofluid droplet sorption in dry powder beds



Timothy Munuhe^a, Alexander Lebrun^b, Liang Zhu^a, Ronghui Ma^{a,*}

^a Department of Mechanical Engineering, University of Maryland Baltimore County, 1000 Hilltop Circle, Baltimore, MD 21250, United States

^b Department of Science, Engineering, and Technology, Howard Community College, 10901 Little Patuxent Parkway, Columbia, MD 21044, United States.

ARTICLE INFO

Article history:

Received 19 April 2016

Received in revised form 21 September 2016

Accepted 27 September 2016

Available online 28 September 2016

Keywords:

Droplet spreading

Droplet sorption

Powder bed wetting

Micro-CT imaging

ABSTRACT

Liquid droplet sorption in dry porous media is an important process for a wide range of scientific and engineering applications. However, visualizing droplet sorption is difficult due to the opacity of the porous media used in most of the applications. In this study, micro-CT technology is used to characterize the sorption profiles of nanofluid droplets in PMMA powder beds. Scan results reveal that the region of the powder bed wetted by the nanofluid has substantially higher pixel index values than the dry powder, thus enabling visualization of the sorption profile. The wetted regions themselves consistently have semi-spheroid shapes with craters on the top surface. The craters may be induced by powder repacking rather than droplet inertia ejecting well-settled powder particles. The sorption of multiple droplets maintains the features of a single droplet granule but increases the lateral spreading more than the penetration in the vertical direction. The inhomogeneous distribution of the pixel index value suggests accumulation of the nanofluid near the wetting front due to inhomogeneous porosity in the wetted region of the powder bed. It is considered that droplet sorption and capillary force may cause the powder particles to repack to generate a low porosity in the center of the wetted region. Nanoparticle distribution in the powder bed after complete evaporation of the nanofluid was also visualized. In conclusion, nanoparticle-enhanced micro-CT imaging has demonstrated the feasibility to visualize three-dimensional sorption profiles of a fluid in dry porous powder beds and thus provided an efficient means to study the sorption process in an opaque porous medium. We also envision that micro-CT can be utilized to characterize nanoparticle distribution in porous media in applications where nanomaterials are introduced for additional functionality of the final products.

© 2016 Published by Elsevier B.V.

1. Introduction

Liquid droplet sorption in dry porous media is an important physical process in a number of applications, including inkjet printing [1–3], oil and gas production [4], and pharmaceutical production [5,6]. More recently, it has received growing attention in 3D powder bed printing, a process that utilizes ink-jet printing technology to create 3D printed parts from layers of powder [7–9]. In this process, droplet sorption behavior plays an important role in determining a number of characteristics of the 3D-printed part [8] such as feature resolution and surface texture [7–9].

The droplet spreading and sorption behavior in a dry porous medium, represented by sorption time, spread diameter and penetration depth, is affected by a wide range of process parameters, including the droplet impact speed, liquid viscosity, powder bed characteristics, wettability of the liquid on the porous medium, and interactions between the droplets in the case of multiple droplet impingement [7]. A prominent focus of previous studies has been the dynamics of a droplet impacting the surface of a porous medium [2,6,10–16]. These

investigations generally record the evolution of the droplet profile using high speed photography, specifically examining the evolution of spread diameter, the height, and the contact angle at the contact line over time. These spreading characteristics are then used to measure the volume loss over time from the drop above the porous medium to the wetted region inside the porous media. For a range of Weber numbers from 10 to 2000 [17], the droplet experiences spreading, retraction and sorption. Splashing and formation of craters are observed for high impact velocities [12,17,18]. Emady et al. [19,20] studied the interaction between drop deformation and powder particle granulation and identified three different granule formation mechanisms: tunneling, spreading, and crater formation, as well as the associated process conditions.

The sorption of a droplet in porous media is mainly driven by the capillary force and resisted by viscous dissipation [1,15,21]. The capillary force on a wetting front, expressed by the capillary pressure, is evaluated theoretically as:

$$p_c = \frac{2\sigma \cos\theta}{r_p} \quad (1)$$

where σ is the surface tension, and θ is the contact angle. In Eq. (1), $r_p = 2\varepsilon / [(1 - \varepsilon)S_0\rho_s]$ is the effective radius of the pores in the bed, where ε is

* Corresponding author.

E-mail address: roma@umbc.edu (R. Ma).

the porosity, s_0 is the particle specific surface area, and ρ_s is the packing density of the pores [12]. Sorption is dependent on the droplet spreading above the surface, the surface tension and viscosity of the liquid, the porosity and permeability of the substrate, and the wettability of the liquid on the solid structure. A number of studies have used sorption time and maximum spreading diameter to characterize the sorption process [5–7,16,22,23]. Hapgood et al. [15] proposed a two-phase model to consider the presence of macrovoids in irregular packing. D'Onofrio et al. [24] performed both experimental and numerical studies to investigate the spreading of liquid in medium grain-size sand after sorption is completed.

Despite extensive studies of droplet impact on dry granular powder beds, information on the sorption profile and interaction between the liquid and unconsolidated powder particles is limited. In particular, it is unclear to what extent liquid infiltration in powder may lead to repacking of the powder particles and subsequently change the porosity of the powder bed. A major challenge in the study of droplet sorption is the difficulty in fully characterizing the wetted region in the powder bed. In most cases, the powder bed is opaque and, therefore, visualization of the final sorption profile has been very limited [25]. Droplet sorption in porous media has been visualized in optically transparent porous media [26] and in thin substrates where sorption is negligible in the out-plane direction [1,27–30]. Reis et al. [31,32] used MRI to obtain the shape of the wetted volume and studied the evaporation process. However, the MRI-imaged sorption profile is two-dimensional and information on the possible repacking of the powder particles is not available.

In recent years, nano-sized materials have enabled important advancements in a wide range of scientific and engineering applications [33,34]. With the rapid development of nanotechnology, the distribution of nanoparticles in porous media after sorption of nanofluid droplets is of special interest due to their technical relevance, as well as their potential risk to the ecosystem and human health [35,36]. However, understanding of the fate of nanoparticles after sorption and evaporation of the liquid in dry porous media is scarce.

In light of the limited investigation of droplet sorption behavior using direct visualization techniques, the goal of this study is to use available micro-computed tomography (micro-CT) technology for the visualization of the final three-dimensional sorption profile of a nanofluid droplet to obtain qualitative information on the repacking of the powder particles. It would also be advantageous to get information on the nanoparticle distribution in a dry powder bed after absorption and evaporation of nanofluid droplets. Our hypothesis is that the liquid in the porous media reaches quasi-steady state after the completion of droplet sorption, and therefore, the saturated volume of the porous medium can be characterized by micro-CT imaging. In this study, droplets of a dilute ferrofluid were dispensed onto homogeneous PMMA powder beds with known powder size distribution. After sorption was complete, these powder beds were then scanned using a micro-CT scanner. Finally, the scan data were post-processed, and image intensity distributions of the scanned images were analyzed to obtain information on the shape and size of the wetted region, the change in powder porosity, and the nanoparticle distribution.

2. Materials and methods

The particles used in the experiment were PMMA microspheres with a reported density of 1.2 g/cm³ and a diameter range of 125–135 μm (Cospheric, LLC, Santa Barbara, CA). The powder beds were prepared by pouring PMMA microspheres into cylindrical cavities drilled into styrofoam blocks. The cylindrical cavities in the styrofoam were 0.5 in. in diameter and in depth. The blocks were 2 \times 0.75 \times 0.75 in. in dimensions, small enough to fit on the platform of the micro-CT scanner used. The powder beds were then tapped lightly and repeatedly to promote repacking and also to ensure a uniform and level surface. This method was used in successive experiments to produce repeatable packing of the powder. The powder used was newly acquired at the

time of the experiments and the experiments themselves were conducted within one day of each other. This assured us that no changes in the surface chemistry of the particles, due to exposure to the atmosphere, had occurred by the time the experiments were completed.

The porosity of the powder bed was characterized by measuring the mass of the powder that fills a known volume of space in a container. Powder was poured into four test tubes to a volume of 2 mL and tapped to settle the particles and level the surface, just as the powder beds were in the saturation experiments. The masses of the powder beds were then measured. Using the density of PMMA microspheres reported by the manufacturer, the porosity of dry powder ε_d is calculated as:

$$\varepsilon_d = 1 - \frac{m_p}{\rho_p V_m} \quad (2)$$

where ρ_p is the density of the PMMA spheres, and V_m and m_p are the measured volume and mass of the powder, respectively. The porosity of the tapped PMMA powder beds is 0.39 ± 0.002 over the four powder beds tested experimentally.

In addition to dry powder, the porosity of the powder saturated with water was also characterized. Measured volumes of water (V_t) were poured in four individual powder-filled test tubes until the powder beds were oversaturated. The test tubes were then shaken with a vortex mixer (MiniRoto Vortexer Shaker, Fisher Scientific, Springfield, NJ) to promote full sorption of the liquid in the powder bed. Finally, the saturated powder was allowed to settle and measurements were taken of the total volume of the powder/liquid mixture (V_t) and saturated powder bed volume (V_p). The latter was determined by the liquid/powder interface. The net volume of the solid particles can be calculated by: $V_s = V_t - V_t$, and the saturated powder bed porosity ε_s is determined by

$$\varepsilon_s = 1 - V_s/V_p. \quad (3)$$

The saturated porosity of the powder bed was measured to be 0.30 ± 0.01 for the four tests. The properties of the PMMA powder are summarized in Table 1. It should be noted that water was used to measure the saturated porosity rather than nanofluid because the liquid/powder interface is invisible due to the dark color of the ferrofluid. As the ferrofluid is water-based, we consider water as an appropriate substitute. We also assume that the presence of nanoparticles has a negligible effect on the packing of the PMMA particles in the liquid owing to its small size and low volumetric concentration.

The nanofluid used in this study is a commercially available ferrofluid (Ferrotec® EMG 700 Series, 5.8 vol% nanoparticles) with its properties given in Table 1. It is a dilute water-based ferrofluid with a nominal particle diameter of 10 nm. Such a small particle size allows us to assume that the nanoparticles catch up with the local fluid velocity instantaneously [37], and therefore, can be used as an indication of the location of the wetting front in the dry powder bed. We also consider that change of the fluid properties by the added particles is negligible due to the low volume fraction of the particles. Most importantly, this particular type of nanofluid has been used in our previous studies of imaging nanoparticle distribution in mouse tumors using micro-CT [38]

Table 1
Properties and parameters.

Properties and parameters	Values
Ferrofluid density (kg/m ³)	1290
Ferrofluid viscosity (mPa·s)	1–5
Ferrofluid surface tension (N/m)	0.051
Nominal nanoparticle size (nm)	10
Nanoparticle density (kg/m ³)	5240
PMMA powder particle size (μm)	125–135
PMMA particle density (kg/m ³)	1200
Contact angle of water on PMMA	68° [39]

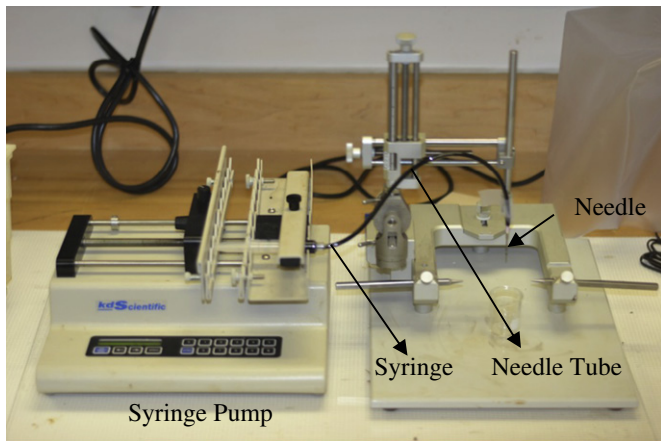


Fig. 1. Experimental set-up.

and has performed satisfactorily. Owing to these reasons, it was decided to be the most appropriate candidate for the study.

Droplets were formed using an 18 gauge Hamilton beveled-tip needle (Fischer Scientific, Springfield, NJ) connected to a 10 cm³ syringe. The syringe was connected to a syringe pump (Genie Plus, Kent Scientific, Inc. Torrington, CT), as shown in Fig. 1. The needle was fixed and positioned so that the needle tip is above the powder bed surface at approximately 5 mm to limit the effects of impact on sorption [20]. Assuming that the droplets dispensed have a spherical shape, the droplet diameter D_0 and volume V_0 are determined to be 2.8 mm and 10.3 μL , respectively, from measurement of the total volume of 30 droplets dispensed at the same flow rate of the syringe pump.

Based on the droplet size and height at which it is released, the droplet impacts with a vertical velocity $u_i \approx \sqrt{2gh} = 0.21\text{m/s}$, where g is the gravitational acceleration, and h is the distance between the needle tip and the bed surface. The main dimensionless parameters used to characterize the impact are the Weber number (We), Bond number (Bo), and Ohnesorge number (Oh). The Weber number, $We = \rho D_0 u_i^2 / \sigma$, where ρ is the nanofluid density and D_0 is the droplet diameter, is estimated to be 7. The Bond number for this study, $Bo = \rho g D_0^3 / \sigma$, is 2, and the Ohnesorge number, $Oh = \mu / \sqrt{\rho \sigma D_0}$, varies in the range of 0.002 to 0.01. The contact angle of water and PMMA is roughly 68° [39]. The wetting properties of the ferrofluid on PMMA are unclear.

Two cases were tested: single droplet and triple droplet sorption in powder beds. In the latter case, three droplets were dispensed to impact

the same location in succession. Three trials of each case were conducted. For the first two trials, the powder beds with adsorbed droplets were scanned twenty minutes after the sorption was complete. For the final trial of each case, scanning was performed after 24 h. To ensure consistency, all the experiments were conducted in air-conditioned laboratories with ambient temperature of 21–23 °C and humidity of 60–69%.

Scans were conducted using a high-resolution micro-CT imaging system (Skyscan1172 Micro Photonics, Inc., Allentown, PA). Each scan took about 40 min. During the process, the de-ionized water served as a baseline for calibrating the scanning parameters. A medium resolution scan of 17 μm (pixel size) was selected and all samples were scanned using the same parameters of 100 KV and 100 μA without a filter. The images acquired through the micro-CT scan were reconstructed using NRecon® software, which is part of the micro-CT imaging system, and image stacks were generated with ImageJ image processing software (developed at the National Institutes of Health). In the scanned images and reconstructed images, the brightness is represented by pixel index numbers between 0 and 255. A typical micro-CT scan of a powder bed may result in a total of 1200 individual images, with each image having a resolution of 1000 \times 524. These images were used to generate a single file that gives the pixel index values in the form of a 3-D matrix using the software SAS 9.4 (SAS Institute Inc., Cary, NC). The resulting pixel index value distributions were plotted with MATLAB R2014a (Mathworks, Natick, MA). The data post-processing was aided by the use of the iso2mesh MATLAB toolbox [40], a set of functions used for processing and analysis of grayscale data and images from MRI and CT scanners.

3. Results

3.1. Nanofluid sorption profile in a powder bed after single droplet sorption

A nanofluid sorption profile after single droplet sorption was observed from the scanned images of all the samples. Fig. 2 provides the side views of the pixel index value distribution on two vertical center planes of the powder bed for the first trial of the single droplet sorption case.

These perpendicular planes were randomly selected. The dry PMMA powder is shown with a pixel index value below 50, while the region wetted by the nanofluid displays a higher value. This is because the iron-based nanoparticles have a significantly higher density (5240 kg/m³) than the PMMA powder. The boundary of the sorption region is marked by elevated pixel index values, with the highest close to 200. The sorption profiles on both planes exhibit a nearly semi-spheroid shape with a similar maximum spread width. A crater can be observed

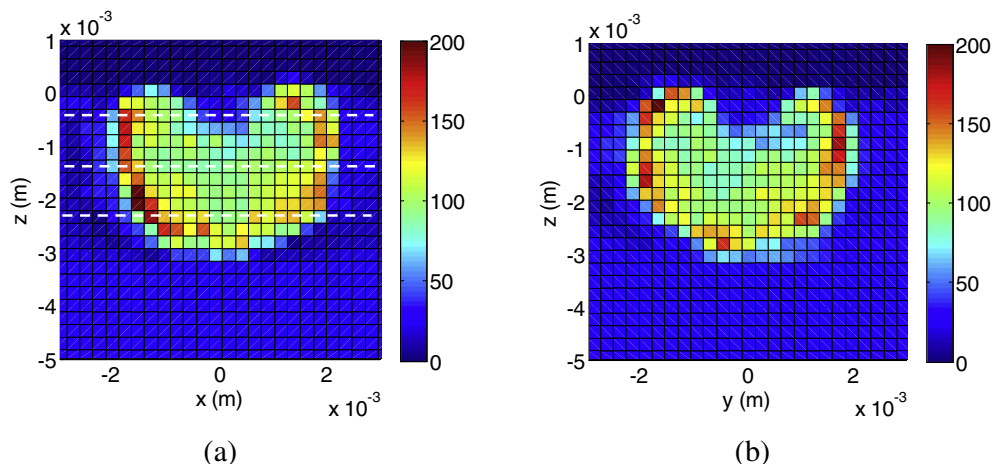


Fig. 2. Side views of pixel index distribution on two vertical center planes perpendicular to each other. These two planes are chosen randomly.

on the top of the sorption profile. Shown in Fig. 3 are the pixel index value distributions on the horizontal planes that are 2.5, 1.5 and 0.5 mm beneath the powder bed surface (marked in Fig. 2a) for trial 1 with a single droplet.

Consistent with the observation on the vertical planes, the area wetted by nanofluid has a nearly circular shape that stems from isotropic droplet spreading on the powder bed. The plane located 1.5 mm beneath the surface has the maximum spread diameter. Using a cutoff pixel index value of 50, the three-dimensional shape of the sorption

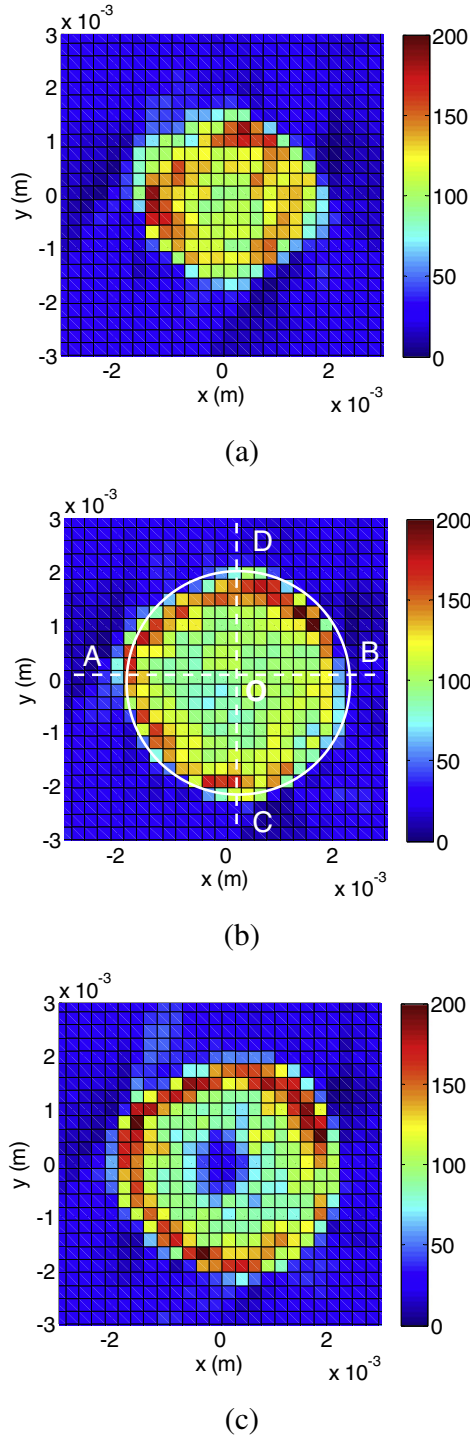


Fig. 3. Pixel index distributions on horizontal planes that are (a) 2.5 mm (b) 1.5 mm and (c) 0.5 mm beneath the top surface, respectively, as marked in Fig. 2a for trial 1 of single droplet sorption.

profile for the first single droplet trial is given in Fig. 4(a). The sorption profiles for trial 2 and 3 show similar patterns for the pixel index value distribution.

3.2. Nanofluid distribution in a powder bed after triple droplet sorption

The patterns of pixel index value distributions for the triple droplet are also obtained from the scanned images. Shown in Fig. 5(a) and (b) are the distributions of pixel index values on two vertical center planes perpendicular to each other for trial one of the triple droplet sorption case.

Corresponding pixel index distributions on horizontal planes 2.8, 1.8 and 0.8 mm beneath the surface are presented in Fig. 6.

Consistent with the single droplet sorption, the boundary of the wetted region is marked by elevated pixel index values. The three-dimensional shape of the sorption profile is presented in Fig. 4(b) using a cutoff pixel index value of 50. Like the single-droplet case displayed in Fig. 3, the triple-droplet case also exhibits a nearly circular spreading pattern on the horizontal planes, and a semi-circular shape when viewed from the side. A crater is observed on the top surface where the droplet impacts. The scanned images for trials 2 and 3 have similar distribution patterns.

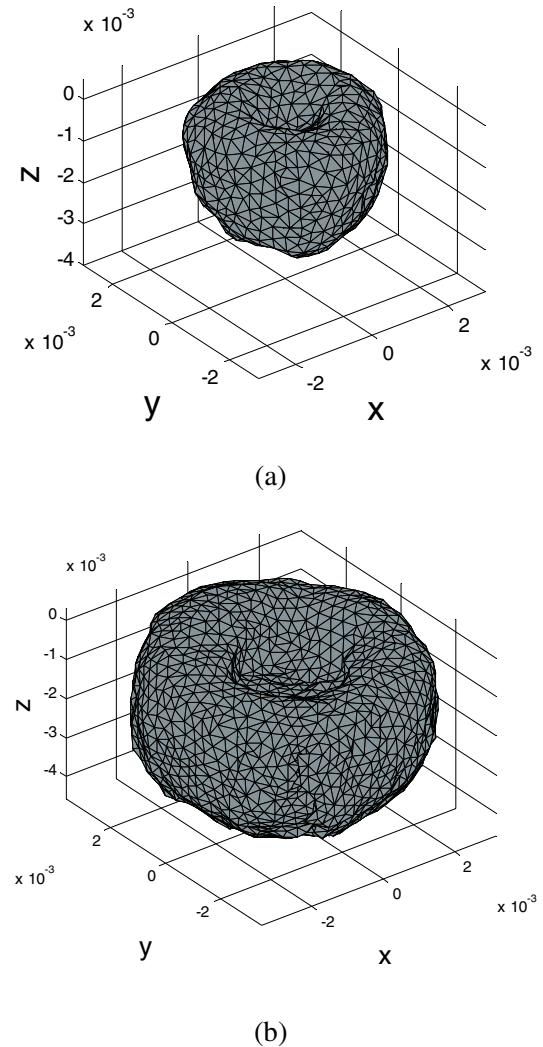


Fig. 4. Isosurface with triangular mesh of wetted region using a cutoff value of 50 for (a) single droplet case, trial 1, and (b) triple droplet case, trial 1.

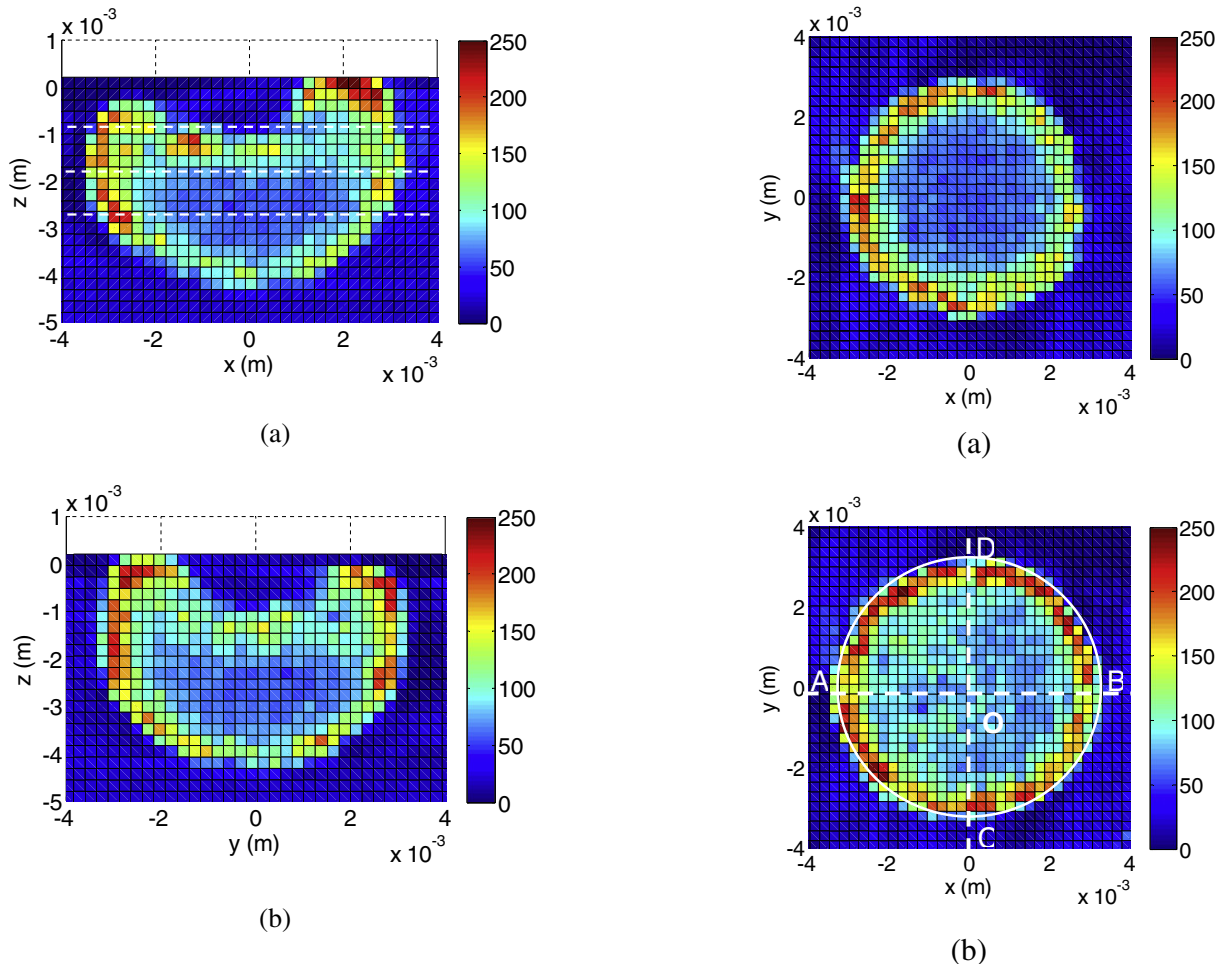


Fig. 5. Side views of pixel index distributions on two vertical center planes perpendicular to each other. These two planes are chosen randomly.

3.3. Nanofluid distribution in a powder bed scanned 24 h after sorption

In the third trials of both cases, the powder beds were scanned 24 h after droplet sorption. Under the humidity and temperature of laboratory conditions, a single droplet deposited on a surface evaporates completely after 4 h. It is thus, reasonable to assume complete evaporation of nanofluid in the powder bed after being exposed to an open environment for 24 h. Displayed in Figs. 7 and 8 are the discrete index values along two perpendicular lines on the horizontal plane of the maximum diameter (Figs. 3b and 5b) for the single and triple sorption, respectively. Presented in the same plot are the averaged pixel index distributions in the radial direction along these two lines. All pixel index value distributions, regardless of the number of droplets absorbed and the lag time before scanning, exhibit the same pattern in the radial direction. Within a large region near the center, the average pixel index value is between 90 and 100. Then they reach a peak value at the boundary. For the triple droplet case, the highest pixel value near the edge is between 200 and 250, while the peak value for the single droplet case is between 160 and 180. The evaporation of the nanofluid in the powder does not appear to cause obvious changes in the pattern of pixel index distributions; however, the widths of the sorption regions after evaporation are smaller. A schematic diagram of the sorption profile on the vertical center plane is shown in Fig. 9 to illustrate the typical features of the wetted region and important geometric parameters.

Based on the acquired data, important geometric dimensions, such as the volume of the wetted region, maximum diameter and penetration depth, aspect ratio, and crater diameter and depth, are also determined and given in Table 2. Assuming the wetted region with a

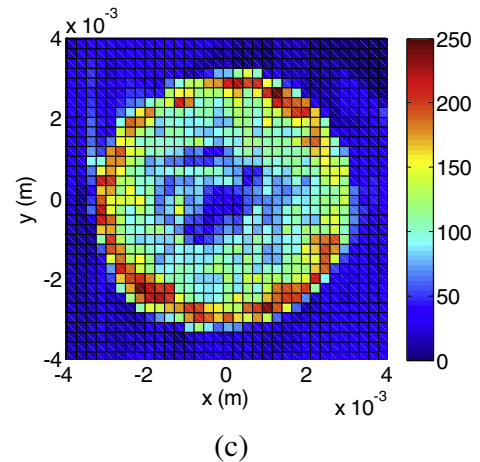


Fig. 6. Pixel index distributions on horizontal planes that are (a) 2.8 mm (a), (b) 1.8 mm and (c) 0.8 mm beneath the top surface, respectively for trial 1 of triple droplet sorption.

volume of V_w to be saturated with nanofluid, the average porosities of the wetted region can then be calculated as V_d/V_w , where V_d is the volume of the dispensed nanofluid. Based on a single droplet volume of $10.3 \mu\text{L}$ and the cutoff pixel index value of 50, the porosities in the wetted region are 0.28–0.30 for the samples scanned 20 min after droplet sorption, as listed in Table 2. The estimated porosities are close to the measured powder porosity when saturated with water.

As expected, the triple droplet case shows a larger saturation volume, which is evidenced by a greater maximum diameter and sorption

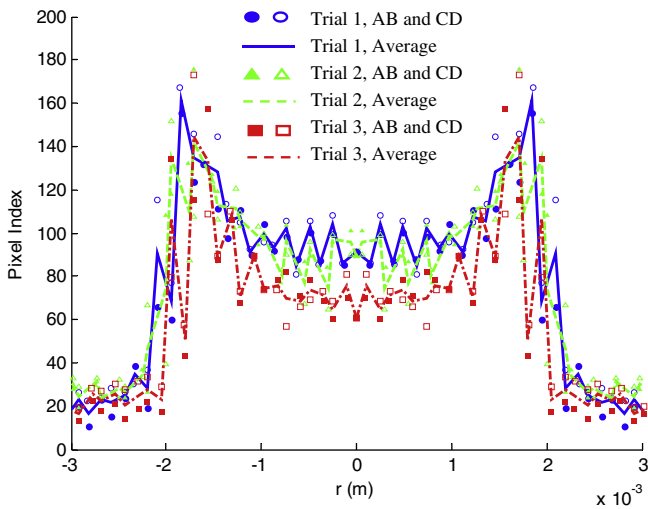


Fig. 7. Variations of pixel index values along AB and CD shown in Fig. 3b for single droplet sorption. The averaged variations of pixel index values in the radial direction over OA, OB, OC, and OD are also plotted.

depth. Triple droplet sorption also yields a large crater diameter and depth. While the single droplet case has a spreading-to-sorption ratio of 4:3, the same ratio for the triple droplet case is 3:2. This suggests that upon the subsequent sorption of the second and third droplets, spreading is facilitated by pre-wetting. The sorption time for a single droplet was shorter than the time between droplet dispensations, meaning multiple droplets interacted above the porous medium surface. Comparison of the crater diameters also supports the idea of above-surface droplet spreading. While the average single droplet crater diameter is 2.6 mm, the average triple droplet crater diameter is 4.3 mm, with a variation of 12%. This increase suggests that lateral spreading inside the porous medium is assisted by the interactions of the droplets above the porous medium, in addition to the pre-wetting of the powder bed by the first droplet. The nanofluid sorption regions of the samples scanned after evaporation show smaller volumes, spread diameters, sorption depths, and lower aspect ratios.

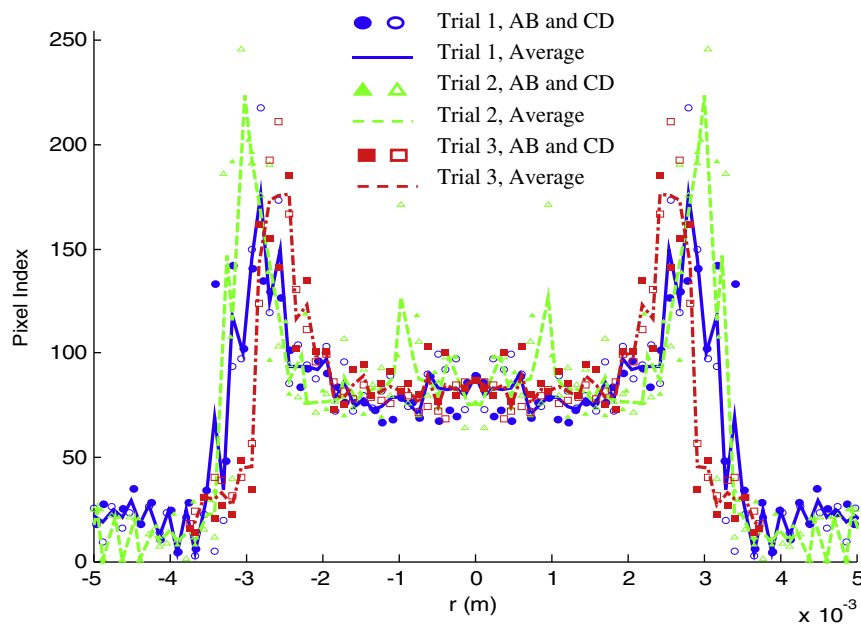


Fig. 8. Variations of pixel index values along AB and CD shown in Fig. 6b for triple droplet sorption. The averaged variations of pixel index values in the radial direction over OA, OB, OC, and OD are also plotted.

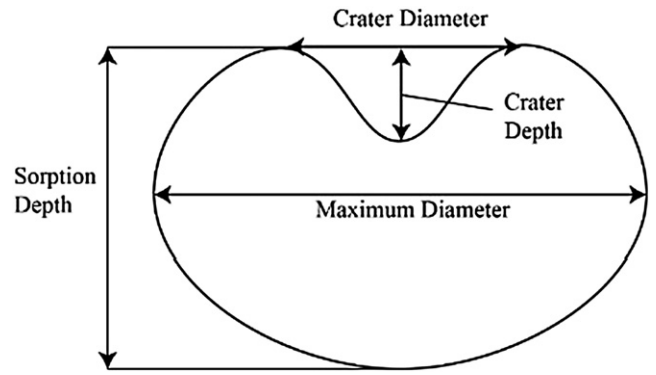


Fig. 9. Important parameters of wetted region.

4. Discussion

Droplet sorption profiles in dry PMMA powder beds are imaged using micro-CT with enhancing agents of iron-based nanoparticles with their density substantially higher than that of water and the PMMA particles. The pixel index values can be considered as an indicator of nanoparticle distribution as they reflect the local density of the scanned medium [38]. A very important issue for nanofluid infiltration in the porous media is the possible deposition of the particles on the solid structure along their path due to strong surface forces such as the van der Waals force and electrostatic force. However, nanoparticle deposition is not obvious in this study because the highest pixel index value is observed on the wetting boundary rather than the region near the top surface. The absence of nanoparticle deposition can be explained by the surfactant coating on the particles that yields a negative charge to prevent particle agglomeration. As PMMA particles also possess a negative charge in the aqueous solution, the repulsive force tends to block the particle attachment to the solid structure.

With negligible nanoparticle deposition on the solid structure, the nanofluid concentration in the pores of the powder bed can be considered constant. Thus, the only explanation for the varying pixel index values observed in a wetted region is the non-uniform porosity after droplet sorption. Thereby, the pixel index values can be considered as

Table 2
Geometric parameters and properties of wetted regions.

Droplet, trial	Wetted volume, V_w (μL)	Estimated granule porosity, ε	Maximum diameter, D (mm)	Sorption depth, H (mm)	Aspect ratio (D/H)	Crater diameter (mm)	Crater depth (mm)
Single, trial 1	34.0	0.30	4.5	3.3	1.36	2.6	0.71
Single, trial 2	36.2	0.29	4.6	3.5	1.31	2.6	0.71
Single, trial 3	25.2	N/A	4.0	3.2	1.25	2.1	0.83
Triple, trial 1	109.3	0.28	6.7	4.5	1.49	4.5	0.71
Triple, trial 2	105.1	0.29	6.8	4.5	1.51	4.0	0.83
Triple, trial 3	71.3	N/A	6.0	4.1	1.46	4.0	0.83

an indicator of local porosity of the powder bed. The distributions of the pixel index value on both vertical and horizontal planes show a more compact core of a semi-spheroid surrounded by a more porous layer of powder filled with nanofluid.

Another explanation for the high pixel index value on the outer surface of the wetted region is the accumulation of nanoparticles on the surface of the droplet due to capillary force. The nanoparticles used in this study are hydrophilic. If significant amounts of nanoparticles assemble on the surface of the droplet, then the top surface of the crater should be marked with pixel index values equivalent to those at the peripheral surface of the wetted region. However, in all scans of single droplet sorption, the peripheral surface shows much higher pixel index values than the top layer. Thereby, we consider that nanoparticle accumulation on the droplet surface is not the leading cause of the observed pattern of pixel index value distribution. Future study should be conducted to examine the effect of nanoparticle accumulation on the droplet surface.

The formation of craters on powder surfaces has been discussed extensively for the case of high impact velocity droplets on loose powder beds consisting of larger-sized powder particles [12,19]. Loose powder particles can be displaced by the high inertia of the liquid to form a crater. For an impact with a low Weber number, only a very shallow crater is observed by Marston et al. [12]. In our study, the Weber number is small, and no obvious powder displacement was observed during droplet impact and spreading. We speculate that the crater formation and heterogeneous porosity might be explained by the loose packing of the top layer PMMA particles and repacking of the PMMA particles driven by capillary forces.

First, the powder particles near the top surface might be compressed to form a shallow crater during the nanofluid sorption due to a possible looser packing of the powder particles in the top layers than average, as illustrated in Fig. 10 (a) and (b). Another important driving force to form the crater is the capillary force at the liquid-air interface. As the ferrofluid partially wets PMMA, the meniscus exerts an inward pulling force on the powder particles that tends to compress the particles, as illustrated in Fig. 10(c). Near the top surface, the compression is facilitated by drag and gravity, leading to a more compact powder and lower local porosity. However, near the wetting front inside the powder bed, the inward capillary force is counteracted by the outward advancement of the liquid, and the repacking of the powder particles is less profound as illustrated in Fig. 10(c). The medium with larger pore size near the wetting front allows more nanofluid to accumulate than the center region and gives rise to sharply elevated pixel index values near the wetting boundary as shown in the imaged sorption profiles. The abrupt increase of the porosity near the wetting front also explains the final steady state of the sorption in the powder. When a liquid advances into the powder by flowing down successively through pores, only pores with increasing diameters can cause the fluid velocity to slow or cease to advance due to the reduced meniscus curvature of the liquid. To summarize, the repacking of the powder particles is supported by the following observations in the experiment: elevated pixel index values near the wetting front inside the powder bed, the porosity of the wetted region close to the saturated porosity, and the steady state final sorption profiles in the PMMA powder that is partially wetted by this particular ferrofluid.

The sorption profiles of the triple droplet case not only show a larger liquid sorption region, but also a greater aspect ratio of the spreading diameter to sorption depth, and a different porosity distribution. The larger aspect ratio can be attributed to the wider spreading of the second and third droplet after the powder bed absorbs the precedent droplet. Also, a compact packing of the particles occurs some distance below the top surface. We consider this as the result of complicated interactions between the liquid and powder particles during the sorption of the subsequent droplets. Future study is needed to understand the multiple-droplet sorption process.

Nanoparticle distribution in the powder bed after complete evaporation of the droplet is of interest due to its technical relevance to 3D inkjet printing technology using nanofluid binder [33]. We observed a similar pattern of nanoparticle distributions after evaporation as those in the wet powder, but with smaller volumes. This can be explained by two important mechanisms involved in the evaporation of liquid in

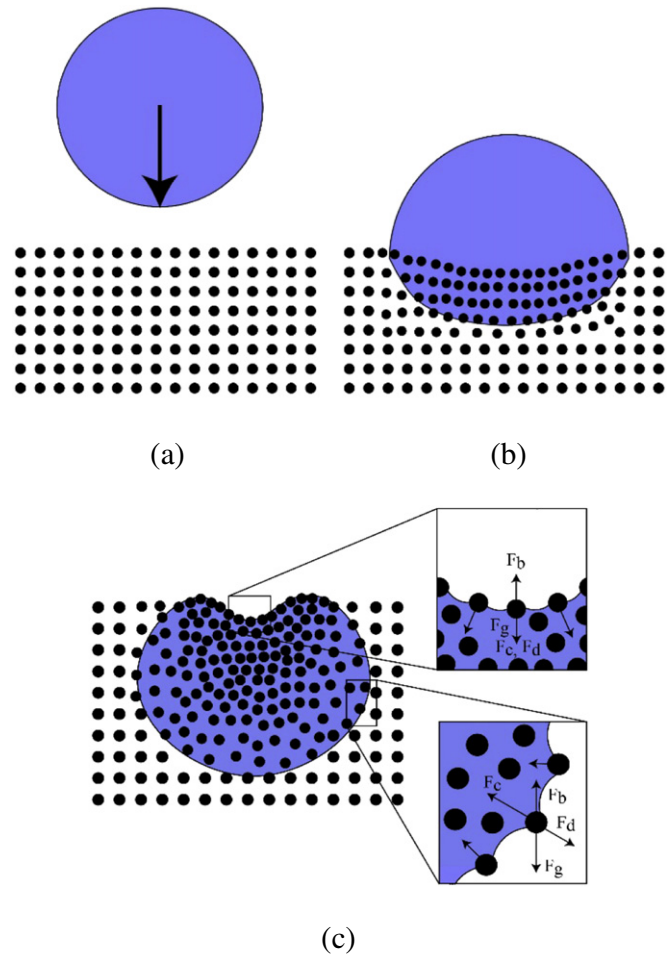


Fig. 10. Impact (a), spreading (b), and sorption process (c). F_c , F_b , and F_d are the capillary force, buoyancy force, gravitational force, and drag force, respectively.

dry porous media. The first stage of liquid evaporation in porous media is characterized by interface recession due to constant evaporation of the liquid at the wetting front. At a certain point, percolation of air into the saturated region occurs, leading air fingers into the sorption region until evaporation is complete. The observed smaller spreading diameter of nanoparticles suggests that nanoparticles recede with the wetting front during the early stage of evaporation until the evaporation is dominated by percolation. In addition to the recession of the wetting front, the nanoparticle distribution is not modified by the evaporation process. The receding distance of the wetting front is submillimeter.

The homogeneity of dry powder is an important issue in the study of droplet sorption in a powder bed. Per the manufacturer's specifications, the PMMA particle sizes follow a Gaussian distribution, with 90% of the particles having a diameter in the range of 125 μm and 135 μm . With regards to the homogeneity of a powder bed, research has been conducted examining the porosity distribution in powder beds [41–44] and has found that significant variation in the porosity is found within three to five sphere diameters from the boundary [42–44] but that there is much less variation beyond this distance. For a powder domain relatively large compared to the powder particles themselves, a single porosity measurement is still commonly used [8,9,45,46]. In this experiment, the powder beds were cylinders with diameters of 1.3 cm. The droplets absorbed at the center of the powder bed had diameters of about 2.8 mm. The maximum spreading diameters of the granules in the study were 4.6 mm for single droplet and 6.8 mm for triple droplet, which are almost two orders of magnitude greater than the powder particles. In addition, the largest droplets spreading diameter of 6.8 mm still gives more than 1 mm on all sides, or 7–8 particle diameters between the wetting front and the wall. Based on these conditions, we consider it reasonable to use one value to characterize the powder bed porosity before droplet sorption.

However, as suggested by previous study, the top layers of the powder, i.e., within 3–5 sphere diameters (which is less than 1 mm in thickness) may have a looser packing than the average even after the powder bed was tapped repeatedly to achieve a compact packing. The looser packing of the top layer may contribute to the formation and unsymmetrical shapes of the craters on the top surface. In addition, there is the possibility of macrovoids appearing in the powder bed which could affect the local porosity and, therefore, sorption behavior [15, 47]. It is assumed that these macrovoids are not numerous because the particular PMMA particles were observed to have good flowability, and the powder beds were tapped, and not simply loosely packed. Lastly, the resulting sorption profiles inside the powder as shown in Figs. 2–6, are fairly consistent in size and shape. The pixel index value distributions on the horizontal planes at different distances from the top surface exhibit nearly homogeneous spreading. Therefore, we consider that the inhomogeneity of the powder bed and the presence of macrovoids have an insignificant effect on the sorption inside the powder bed.

One limitation of the study of repacking in the powder bed using micro-CT imaging is the uncertainty of the level of saturation in the wetted region. Although the calculated average porosity of the nanofluid-absorbed regions is equivalent to saturated PMMA powder in water, the uncertainty associated with the evaluation of the average porosity does not rule out the possibility of partial saturation in the wetted region. More research effort is needed in the future to investigate the effect of partial saturation during droplet absorption. Additionally, the colloidal dispersion used should be fully characterized to investigate its effects on the droplet spreading and sorption if the particles are added solely to enhance imaging with micro-CT. The addition of dispersed nanoparticles to a Newtonian liquid affects the density, the effective viscosity, the surface tension of the overall mixture, and its wetting properties. As the volumetric concentration of the particles is about 5.8 vol%, the dilute suspension can still be approximated as a Newtonian fluid. However, the nanofluid has a higher mass density (1290 kg/m^3) than water and it is expected that nanofluid would experience a higher gravitational force which would increase sorption. Yet the ferrofluid

also has a higher viscosity and lower surface tension than water, as shown in Table 1. The wetting property of the ferrofluid on PMMA is not available and its effect on capillary pressure remains unclear. In the future, the viscosity and surface tension of the ferrofluid, as well as its contact angle with PMMA, should be investigated experimentally to more accurately associate the observed results to the ferrofluid properties.

5. Conclusion

Ferrofluid droplet sorption profiles inside an opaque PMMA powder bed were successfully imaged using micro-CT technology. The presence of the nanoparticles enhances the visualization of the sorption profiles by increasing the density difference between the saturated and dry porous media. The sorption profile itself consists of a nearly semispherical wetting front and a crater at the top surface. The wetted region after the absorption of three droplets shows wider spreading due to pre-wetting of the powder particles.

The distributions of the pixel index value suggest a larger porosity near the wetting front and a lower one at the center. The non-homogeneous porosity in the wetted region is attributed to repacking of the powder particles due to the interactions of surface chemistry, inertia, drag, and capillary force. The results also suggest that nanoparticles are more concentrated near the boundary of the granule than the center before and after evaporation for both single and multiple droplet absorption.

With careful control of the materials used in the study and their properties, future studies on granule morphology may use micro-CT technology to better link process parameters to the shape of the granule. Such investigations will elucidate the best parameters for control of the granulation process of different powders. To the authors' best knowledge, this is the first study of visualizing 3D structures of a granule after droplet sorption. However, quantitative analysis of nanoparticle concentration and the porosity of the repacked powder bed has not been conducted in this study due to the limited range of the pixel index value. Research effort will be continued in the future to examine the effect of added nanoparticles on droplet sorption and quantitatively characterize the microstructure of the saturated region. We envision the current study as the first step towards nanoparticle-enhanced micro-CT imaging and characterization of liquid absorption in dry powder beds and the interactions between liquid and powder particles.

Acknowledgements

Research was partially supported by NSF research grant CBET-1335958. The authors would also like to thank the lab of Ryan J. White at the UMBC Chemistry department for assistance with porosity measurements.

References

- [1] R.C. Daniel, J.C. Berg, Spreading on and penetration into thin, permeable print media: application to ink-jet printing, *Adv. Colloid Interf. Sci.* 123 (2006) 439–469.
- [2] T. Gambaryan-Roisman, Liquids on porous layers: wetting, imbibition and transport processes, *Curr. Opin. Colloid Interface Sci.* 19 (2014) 320–335.
- [3] M. Hilpert, A. Ben-David, Infiltration of liquid droplets into porous media: effects of dynamic contact angle and contact angle hysteresis, *Int. J. Multiphase Flow* 35 (2009) 205–218.
- [4] M. El-Alej, M. Corsar, D. Mba, Monitoring the presence of water and water-sand droplets in a horizontal pipe with Acoustic Emission technology, *Appl. Acoust.* 82 (2014) 38–44.
- [5] K. Hapgood, B. Khanmohammadi, Granulation of hydrophobic powders, *Powder Technol.* 189 (2009) 253–262.
- [6] T. Nguyen, W. Shen, K. Hapgood, Drop penetration time in heterogeneous powder beds, *Chem. Eng. Sci.* 64 (2009) 5210–5221.
- [7] B. Utela, D. Storti, R. Anderson, M. Ganter, A review of process development steps for new material systems in three dimensional printing (3DP), *J. Manuf. Process.* 10 (2008) 96–104.
- [8] K. Lu, W. Reynolds, 3DP process for fine mesh structure printing, *Powder Technol.* 187 (2008) 11–18.

- [9] K. Lu, M. Hiser, W. Wu, Effect of particle size on three dimensional printed mesh structures, *Powder Technol.* 192 (2009) 178–183.
- [10] S.M. Kumar, A.P. Deshpande, Dynamics of drop spreading on fibrous porous media, *Colloids Surf. A Physicochem. Eng. Asp.* 277 (2006) 157–163.
- [11] V. Starov, S. Zhdanov, M. Velarde, Spreading of liquid drops over thick porous layers: complete wetting case, *Langmuir* 18 (2002) 9744–9750.
- [12] J. Marston, J. Sprittles, Y. Zhu, E. Li, I. Vakarelski, S. Thoroddsen, Drop spreading and penetration into pre-wetted powders, *Powder Technol.* 239 (2013) 128–136.
- [13] M. Oostveen, G. Meesters, J. van Ommen, Quantification of powder wetting by drop penetration time, *Powder Technol.* 274 (2015) 62–66.
- [14] R. Holman, M. Cima, S. Uhlend, E. Sachs, Spreading and infiltration of inkjet-printed polymer solution droplets on a porous substrate, *J. Colloid Interface Sci.* 249 (2002) 432–440.
- [15] K.P. Hapgood, J.D. Litster, S.R. Biggs, T. Howes, Drop penetration into porous powder beds, *J. Colloid Interface Sci.* 253 (2002) 353–366.
- [16] A. Clarke, T. Blake, K. Carruthers, A. Woodward, Spreading and imbibition of liquid droplets on porous surfaces, *Langmuir* 18 (2002) 2980–2984.
- [17] E. Nefzaoui, O. Skurtys, Impact of a liquid drop on a granular medium: Inertia, viscosity and surface tension effects on the drop deformation, *Exp. Thermal Fluid Sci.* 41 (2012) 43–50.
- [18] J. Marston, S.T. Thoroddsen, W. Ng, R. Tan, Experimental study of liquid drop impact onto a powder surface, *Powder Technol.* 203 (2010) 223–236.
- [19] H.N. Emady, D. Kayrak-Talay, W.C. Schwerin, J.D. Litster, Granule formation mechanisms and morphology from single drop impact on powder beds, *Powder Technol.* 212 (2011) 69–79.
- [20] H.N. Emady, D. Kayrak-Talay, J.D. Litster, A regime map for granule formation by drop impact on powder beds, *AIChE J.* 59 (2013) 96–107.
- [21] E. Nowak, P. Robbins, G. Combes, E. Stitt, A. Pacey, Measurements of contact angle between fine, non-porous particles with varying hydrophobicity and water and non-polar liquids of different viscosities, *Powder Technol.* 250 (2013) 21–32.
- [22] Z. Zhou, F. Buchanan, C. Mitchell, N. Dunne, Printability of calcium phosphate: calcium sulfate powders for the application of tissue engineered bone scaffolds using the 3D printing technique, *Mater. Sci. Eng. C* 38 (2014) 1–10.
- [23] A. Butscher, M. Bohner, S. Hofmann, L. Gauckler, R. Muller, Structural and material approaches to bone tissue engineering in powder-based three-dimensional printing, *Acta Biomater.* 7 (2011) 907–920.
- [24] T.G. D'Onofrio, H.K. Navaz, B. Markicevic, B.A. Mantooh, K.B. Sumpter, Experimental and numerical study of spread and sorption of VX sessile droplets into medium grain-size sand, *Langmuir* 26 (2009) 3317–3322.
- [25] T.J. Heindel, A review of X-ray flow visualization with applications to multiphase flows, *J. Fluids Eng.* 133 (2011) 074001.
- [26] A. Lembach, I. Roisman, C. Tropea, Drop Impact on Porous Media, *Proceeding of ILASS–Europe 2011, 24th European Conference on Liquid Atomization and Spray Systems, Estoril, Portugal, 2011.*
- [27] V. Starov, S. Kostvintsev, V. Sobolev, M. Velarde, S. Zhdanov, Spreading of liquid drops over dry porous layers: complete wetting case, *J. Colloid Interface Sci.* 252 (2002) 397–408.
- [28] M. Selim, V. Yesavage, R. Chebbi, S. Sung, J. Borch, J. Olson, Drying of water-based inks on plain paper, *J. Imaging Sci. Technol.* 41 (1997) 152–158.
- [29] D. Danino, A. Marmur, Radial capillary penetration into paper: limited and unlimited liquid reservoirs, *J. Colloid Interface Sci.* 166 (1994) 245–250.
- [30] A. Borhan, K. Rungta, An experimental study of the radial penetration of liquids in thin porous substrates, *J. Colloid Interface Sci.* 158 (1993) 403–411.
- [31] N. Reis, R. Griffiths, M. Mantle, L. Gladden, Investigation of the evaporation of embedded liquid droplets from porous surfaces using magnetic resonance imaging, *Int. J. Heat Mass Transf.* 46 (2003) 1279–1292.
- [32] N. Reis, R. Griffiths, M. Mantle, L. Gladden, J. Santos, MRI investigation of the evaporation of embedded liquid droplets from porous surfaces under different drying regimes, *Int. J. Heat Mass Transf.* 49 (2006) 951–961.
- [33] M.D. Chavanpatil, A. Khair, J. Panyam, Nanoparticles for cellular drug delivery: mechanisms and factors influencing delivery, *J. Nanosci. Nanotechnol.* 6 (2006) 2651–2663.
- [34] X. Bai, D. Golberg, Y. Bando, C. Zhi, C. Tang, M. Mitome, K. Kurashima, Deformation-driven electrical transport of individual boron nitride nanotubes, *Nano Lett.* 7 (2007) 632–637.
- [35] T. Masciangelo, W.-X. Zhang, Peer reviewed: environmental technologies at the nanoscale, *Environ. Sci. Technol.* 37 (2003) 102A–108A.
- [36] S.A. Bradford, M. Bettahar, Concentration dependent transport of colloids in saturated porous media, *J. Contam. Hydrol.* 82 (2006) 99–117.
- [37] D. Su, R. Ma, M. Salloum, L. Zhu, Multi-scale study of nanoparticle transport and deposition in tissues during an injection process, *Med. Biol. Eng. Comput.* 48 (2010) 853–863.
- [38] A. Attaluri, R. Ma, Y. Qiu, W. Li, L. Zhu, Nanoparticle distribution and temperature elevations in prostatic tumours in mice during magnetic nanoparticle hyperthermia, *Int. J. Hypertherm.* 27 (2011) 491–502.
- [39] Y. Ma, X. Cao, X. Feng, Y. Ma, H. Zou, Fabrication of super-hydrophobic film from PMMA with intrinsic water contact angle below 90 degrees, *Polymer* 48 (2007) 7455–7460.
- [40] Q. Fang, D.A. Boas, Tetrahedral mesh generation from volumetric binary and gray-scale images, *Biomedical Imaging: From Nano to Macro, 2009. ISBI'09, IEEE Int. Symp., IEEE* (2009) 1142–1145.
- [41] G.E. Mueller, Radial void fraction distributions in randomly packed fixed beds of uniformly sized spheres in cylindrical containers, *Powder Technol.* 72 (1992) 269–275.
- [42] J. Theuerkauf, P. Witt, D. Schwesig, Analysis of particle porosity distribution in fixed beds using the discrete element method, *Powder Technol.* 165 (2006) 92–99.
- [43] C.G.D. Toit, Radial variation in porosity in annular packed beds, *Nucl. Eng. Des.* 238 (2008) 3073–3079.
- [44] M. Suzuki, T. Shinmura, K. Iimura, M. Hirota, Study of the wall effect on particle packing structure using x-ray micro computed tomography, *Adv. Powder Technol.* 19 (2008) 183–195.
- [45] X. Jia, M. Gan, R. Williams, D. Rhodes, Validation of a digital packing algorithm in predicting powder packing densities, *Powder Technol.* 174 (2007) 10–13.
- [46] L. Liu, I. Marziano, A. Bentham, J. Litster, E. White, T. Howes, Effect of particle properties on the flowability of ibuprofen powders, *Int. J. Pharm.* 362 (2008) 109–117.
- [47] A. Hoffmann, H. Finkers, A relation for the void fraction of randomly packed particle beds, *Powder Technol.* 82 (1995) 197–203.